ACS Photonics

pubs.acs.org/journal/apchd5

Article

# Characterization of Extreme Ultraviolet Vortex Beams with a Very High Topological Charge

Alok Kumar Pandey,*,§ Alba de las Heras,*,§ Tanguy Larrieu, Julio San Román, Javier Serrano, Luis Plaja, Elsa Baynard, Moana Pittman, Guillaume Dovillaire, Sophie Kazamias, Carlos Hernández-García, and Olivier Guilbaud

Cite This: *ACS Photonics* 2022, 9, 944–951

Read Online

ACCESS | Metrics & More | Article Recommendations | Supporting Information

**ABSTRACT:** Recent developments of high harmonic generation (HHG) have enabled the production of structured extreme-ultraviolet (EUV) ultrafast laser beams with orbital angular momentum (OAM). Precise manipulation and characterization of their spatial structure are paramount for their application in state-of-the-art ultrafast studies. In this work, we report the generation and characterization of EUV vortex beams bearing a topological charge as high as 100. Thanks to OAM conservation, HHG in noble gases offers a unique opportunity to generate ultrafast harmonic beams with a high topological charge from low charge infrared vortex beams. A high-resolution Hartmann wavefront sensor allows us to perform a complete spatial characterization of the amplitude and phase of the 25th harmonic beam (32.6 nm), revealing very high-topological charges in the EUV spectral regime. Our experimental results, supported by numerical HHG simulations, demonstrate the linear upscaling of the OAM of the high-order harmonics with that of low-charge driving vortex beams, showing the sensitiveness of the OAM content to the purity of the driving beam. The generation of structured EUV beams carrying large topological charges brings in the promising scenario of OAM transfer from light to matter at both macroscopic and microscopic scales.

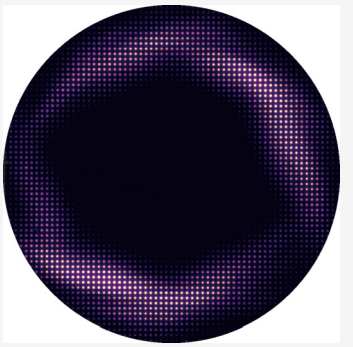

**KEYWORDS:** *structured light, orbital angular momentum, optical vortices, nonlinear optics, high-order harmonic generation, short-wavelength wavefront sensing*



Structured light beams are emerging as a unique tool for the next generation of applications of laser light.[1,2] In particular, our ability to control the spatial phase distribution of laser beams, or their wavefront, allows us to imprint orbital angular momentum (OAM) into light beams. Light beams carrying OAM,[3] also known as optical vortex beams, exhibit a spatially varying phase dependence around the beam propagation axis given by $e^{il\phi}$. The topological charge $l$ designates the number of $2\pi$ phase shifts along the azimuthal coordinate $\phi$ in the transverse plane. The central phase singularity results in a donut-like intensity profile with a null on-axis intensity. Optical vortex beams have proven their utility for a wide range of applications,[4] including optical trapping and tweezing,[5,6] super-resolution microscopy,[7,8] optical communication,[9,10] and quantum information.[11,12] Moreover, with the demonstration of OAM transfer to bound,[13] free electrons[14] and the observation of magnetic helicoidal dichroism,[15] optical vortex beams have brought light−matter interactions to a novel regime.

In the visible, infrared (IR), and long wavelength regimes, helical phased beams can be readily obtained using diffractive and refractive optical elements, such as, but not limited to, a spiral-phase plate (SPP), q-plates, and spatial light modulators.[16] These techniques are highly inefficient in the extreme-ultraviolet (EUV) and X-ray spectral ranges, where the generation of vortex beams is of particular interest, as it offers the possibility of extending their applications down to nanometric spatial and subfemtosecond temporal resolutions. Although already demonstrated at large scale synchrotron and X-ray free-electron laser facilities,[17−19] in the recent past, high-order harmonic generation (HHG) in noble gases has proven to be a handy way to produce EUV vortex beams with configurable topological charge,[20−26] circular polarization,[27,28] and even time-varying OAM,[29] using a table-top setup. A typical HHG spectrum consists of a perturbative region where the intensity exponentially decreases with the harmonic order, followed by a large set of high-orders scaling nonperturbatively with the driving beam intensity.[30,31] In the context of OAM-driven HHG, when a beam of topological charge $l_1$ drives HHG, the topological charge of the upconverted harmonics

**Received:** November 17, 2021
**Published:** February 27, 2022







https://doi.org/10.1021/acsphotonics.1c01768
*ACS Photonics* 2022, 9, 944−951

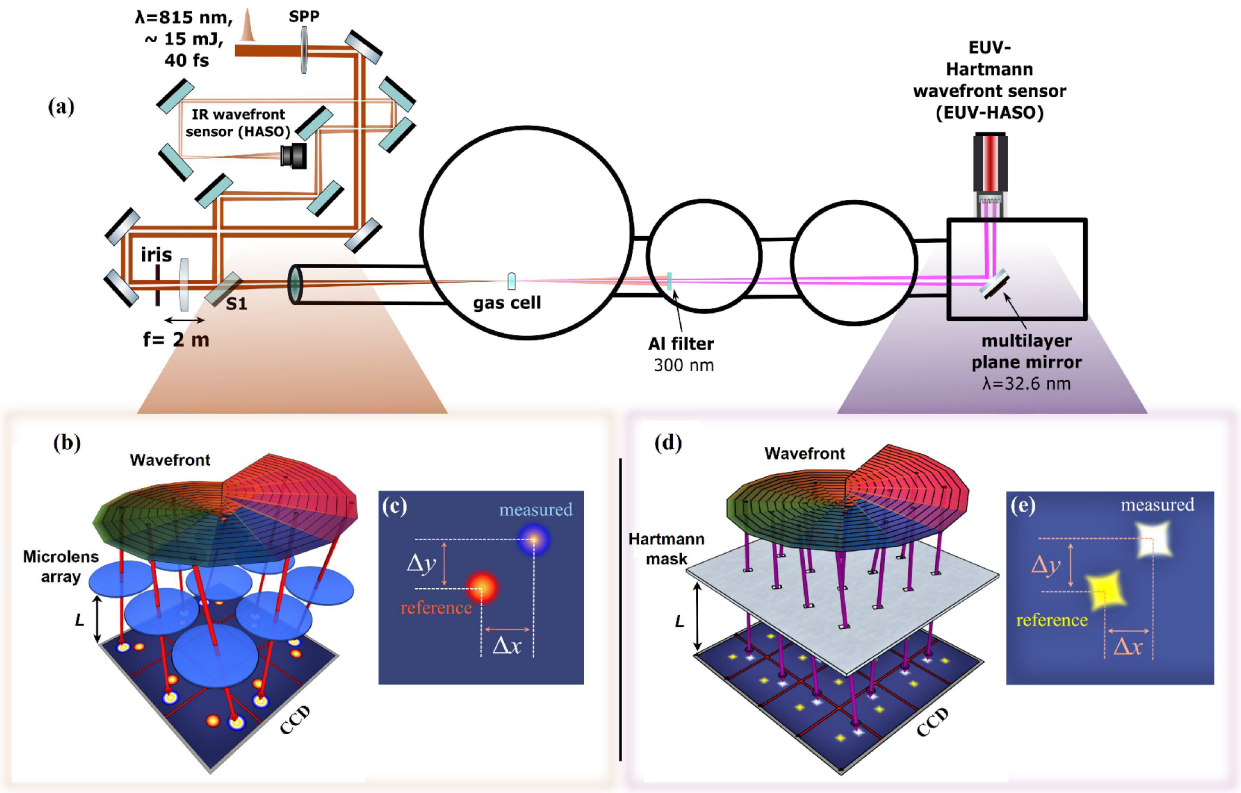


**Figure 1.** Experimental setup for the generation and characterization of EUV vortex beams. (a) A loosely focused IR vortex beam drives HHG in an extended (15 mm long) argon-filled gas cell. The intensity and wavefront of IR and upconverted EUV vortex beams are characterized using Shack−Hartmann (HASO) and Hartmann (EUV-HASO) wavefront sensors, respectively. In the insets of (b)−(e), we show the working principle of IR and EUV wavefront sensors. Each element of the sampling array (microlens in the case of IR-HASO (b) and microhole for EUV-HASO (d)) divides the incident beam into numerous beamlets. Depending on the local wave vector direction, these beamlets are displaced concerning the reference spots of the calibrated wavefront sensor, as shown in (c) and (e). The wavefront is reconstructed from the sampled spot distribution registered on a CCD camera located at a certain distance $L$ from the sampling array (see Supporting Information).

scales linearly with the harmonic order:[21] $l_q = ql_1$, where $l_q$ is the topological charge of the $q^{th}$ harmonic. This linear scaling, which has been experimentally validated for perturbative,[32,33] as well as for nonperturbative, harmonic generation,[22,23,26] results from the energy conservation during frequency upconversion: $\omega_q = q\omega_1$, where $\omega_1$ and $\omega_q$ are the frequencies of the driving and the $q$th order harmonic beams, respectively.

The combination of different vortex driving modes has enabled outstanding control over the properties of harmonic vortex beams. On the one hand, HHG driven by a combination of two vortex beams of different topological charges in a noncollinear geometry leads to an array of spatially separated beams, each carrying a different OAM, and hence, it has provided an additional knob to control the topological charge of EUV vortex beams.[24,25] On the other hand, in a collinear HHG configuration involving two distinct topological charge drivers, theoretical investigations predict a more involved OAM distribution.[34] Indeed, by properly selecting the OAM of the two driving beams, several properties, such as polarization,[27,28] self-torque,[29] and spectral line spacing of high-order harmonic beams,[35] can be tailored. Moreover, the effect of the nonperturbative harmonic intrinsic phase has been studied numerically in ref 34 and can further increase the OAM content. In this regard, a suitable experimental method of characterization is a prerequisite to constructively utilize EUV vortex beams with a broad OAM spectrum or to pave the way toward the generation of high-purity OAM modes.

The characterization of optical vortex beams is a nontrivial task, which becomes even more challenging in the EUV domain. Techniques based on interferometry, diffraction, employing cylindrical lenses, and exploiting dimensional properties of optical vortex beams, have been widely used.[36−40] Some of these methods have also been used to deduce the topological charge of HHG vortex beams.[22,23,25] However, since these methods are unable to measure both amplitude and phase, they often retrieve only the average OAM value. As it is imperative to characterize the complex wavefront of high-harmonic OAM beams for practical applications, these techniques have limited utility. In this sense, Shack−Hartmann and Hartmann wavefront sensors enable a high resolution characterization of both the amplitude and the wavefront of laser beams. Regarding optical vortex beams, it is worthwhile to note that Shack−Hartmann wavefront sensing has been previously used to reconstruct the helical wavefront,[41] to measure the Poynting vector skew angle,[42] and to determine the coherence properties of partially coherent vortex beams.[43] Most recently, the availability of EUV Hartmann sensors has allowed wavefront characterization of topological charge up to 25.[24,26]

In this work, we report the characterization of EUV vortex beams manifesting a topological charge as high as $l$ = 100, which, to the best of our knowledge, represents the highest topological charge measured in the EUV regime. Such extremely high charge vortex beams are obtained through HHG under a loose focusing geometry in an extended argon


https://doi.org/10.1021/acsphotonics.1c01768
ACS Photonics 2022, 9, 944−951

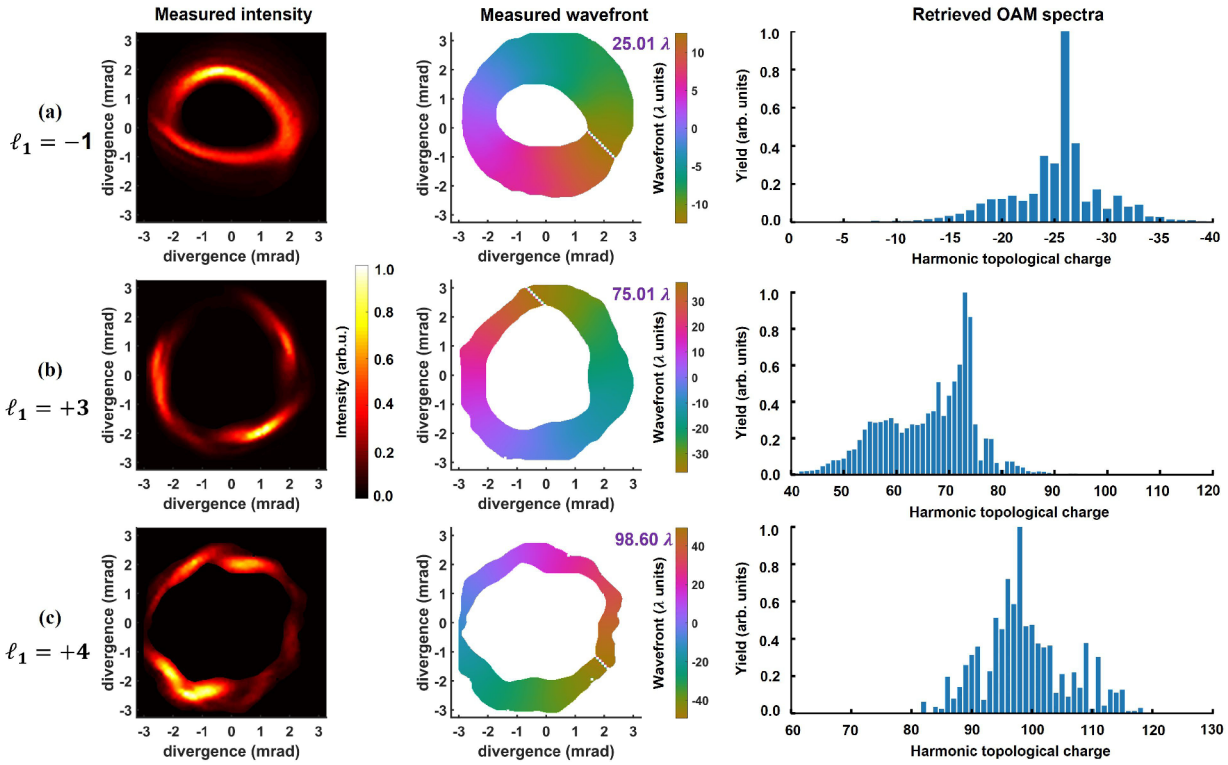


**Figure 2.** Experimental characterization of high topological charge EUV vortex beams. Intensity (left) and wavefront (center) of the 25th harmonic driven by a vortex beam of topological charge (a) $l_1 = -1$, (b) $l_1 = 3$, and (c) $l_1 = 4$. We plot the wavefronts in units of wavelength, $\lambda$, and the peak-to-valley wavefront values are (a) ∼25.01$\lambda$, (b) ∼75.01$\lambda$, and (c) ∼98.6$\lambda$. Though the intensity and wavefront already characterize the harmonic vortex beams, for the sake of completeness, we retrieve the radially integrated OAM spectrum for each case (right) via azimuthal Fourier Transform. The dominant OAM modes are the 26th, 73rd, and 98th for $|l_1| = 1$, 3, and 4, respectively.

gas cell. Moreover, instead of relying on diffractive or interferometric techniques, we exploit both EUV and IR wavefront metrology to fully characterize the intensity, wavefront, and OAM content of the 25th harmonic beam (32.6 nm) and its IR driver (815 nm). By driving HHG with vortex beams with topological charges up to $l_1 = 4$, we show that the EUV vortex beams reach $l_{25} = 100$ as expected, comprising a rich OAM content influenced by the modal purity of the driving beams and the underlying nonperturbative nature of HHG. To further corroborate this observation, we perform advanced theoretical simulations of HHG using the experimentally retrieved IR vortex beam. Our results are general, being relevant not only to upconverted vortex beams obtained via HHG in noble gases, but also from plasma surfaces[44] and semiconductors,[45] where the generation mechanism is known to be nonperturbative.[44,46] Interestingly, ultrafast EUV beams with such a high topological charge open the route to transfer OAM not only to macroscopic particles, but also to clusters or even molecules, bringing in the scenario of light−matter OAM transfer and providing a novel tool to test the correspondence principle between classical and quantum physics for large quantum numbers.

## GENERATION AND CHARACTERIZATION OF HIGH TOPOLOGICAL CHARGE HHG VORTEX BEAMS

We show the experimental setup overview in Figure 1. A more complete description of the setup is provided in the Supporting Information. A linearly polarized near-IR Gaussian beam with an 815 nm central wavelength, ∼40 fs pulse duration full width at half-maximum (fwhm), ∼15 mJ maximum energy, ∼24 mm diameter at $1/e^2$, and a root-mean-square (RMS) wavefront of ∼$\lambda$/32 drives HHG in an extended argon gas cell. The HHG beamline is equipped with IR Shack−Hartmann and high-resolution EUV Hartmann[47] wavefront sensors that allow the wavefront characterization of the IR and the upconverted high-order harmonic beams, respectively. The working principle of the two sensors is illustrated in Figure 1b−e, whereas their characteristics and methodology of wavefront reconstruction are detailed in the Supporting Information. Unlike ptychographic,[48] or other iterative techniques,[49] wavefront sensors offer the possibility of single-shot amplitude and phase characterization. Besides, the sign of the topological charge can be easily determined from the measured wavefront, which allows to distinguish the OAM helicity.

In order to obtain IR vortex drivers, the incoming Gaussian beam is passed through a spiral phase plate (SPP), imparting a helical wavefront. The resulting beam is apertured using an iris with a diameter of ∼18 mm, and it is focused by a 2 m focal length lens to generate high-harmonics in a 15 mm long argon-filled gas cell. A loose-focusing geometry and an extended generation medium allow the production of intense HHG vortex beams, permitting wavefront characterization in a single to few tens of laser shots. After removing the copropagating residual driving beam using a thin metallic filter, the 25th harmonic of the fundamental driver is spectrally filtered using a narrowband multilayer flat mirror, and it is guided to the EUV Hartmann wavefront sensor. Detection of a given harmonic order allows an unambiguous interpretation of the EUV vortex wavefront; extinction of neighboring orders exceeds 90%.[26] The intensity and wavefront are reconstructed from raw


https://doi.org/10.1021/acsphotonics.1c01768
ACS Photonics 2022, 9, 944−951

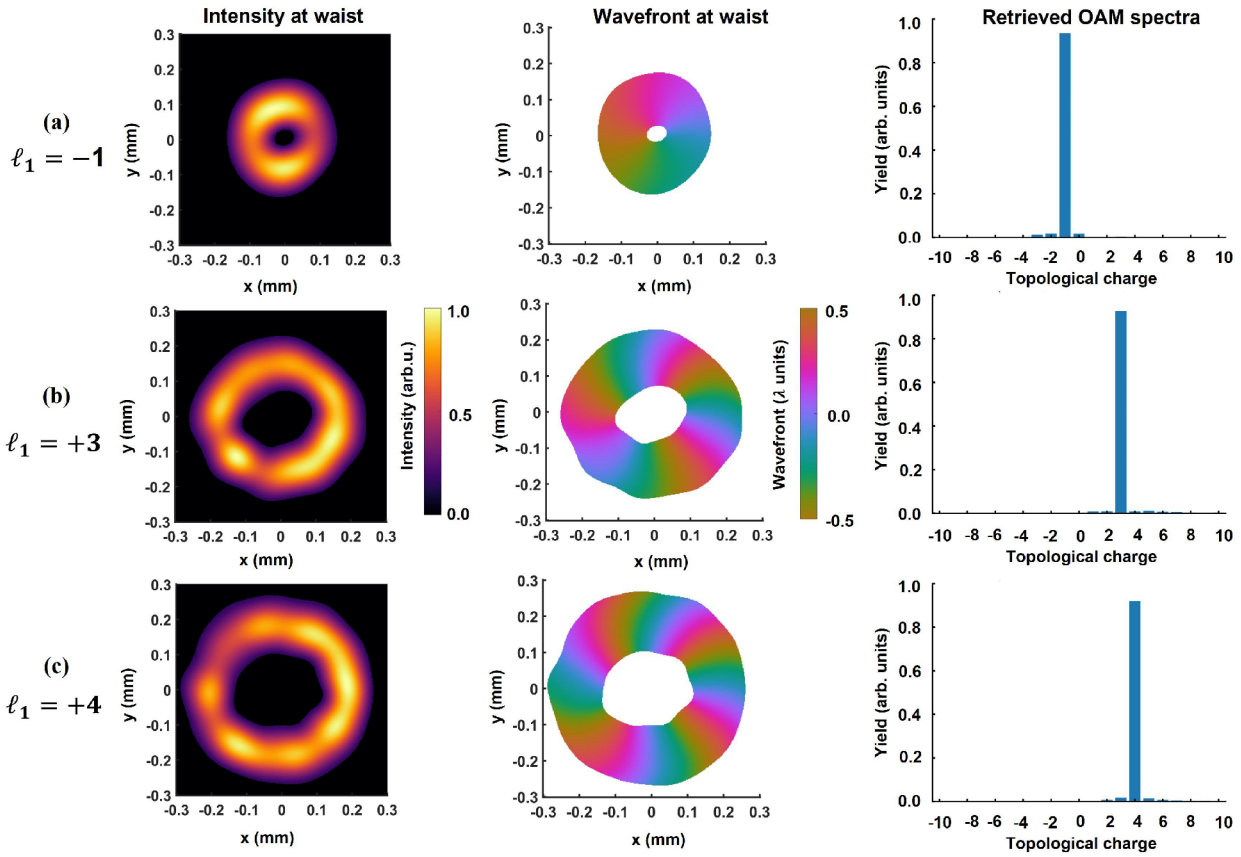


**Figure 3.** IR vortex driver experimental characterization. To facilitate a high spatial sampling of the IR driving beams, the IR wavefront sensor is placed ~300 mm after the focal plane, as shown in Figure 1. The complex field detected by the IR wavefront sensor is backpropagated to the waist. We show the resulting intensity (left), wavefront expressed in the unit of $\lambda$ (center), and radially integrated OAM spectrum (right) for the driving beams of (a) $l_1 = -1$, (b) $l_1 = 3$, and (c) $l_1 = 4$. The radially integrated OAM spectra indicate that the contribution to the desired OAM order is over 90% in all the cases: ~93.4% for $l_1 = -1$, ~92.6% for $l_1 = 3$, and ~92% for $l_1 = 4$.

Hartmanngrams using an iterative algorithm (see Supporting Information).

Figure 2 shows the intensity (first column) and wavefront (second column) of the 25th harmonic beam when driven by an IR vortex beam with (a) $l_1 = -1$, (b) $l_1 = 3$, and (c) $l_1 = 4$. The wavefront is represented in units of the central wavelength of light. Note that the positive (negative) sign of the topological charge indicates the clockwise (anticlockwise) rotation of the wavefront. An annular intensity profile, although irregular, along with a continuous and smooth wavefront rotation are observed for all the configurations. The total wavefront twist around the intensity ring, which is the peak-to-valley (PtV) wavefront value, points out the overall topological charge of the vortex beam. Resulting from the OAM conservation,[21] for the driving beams of $l_1 = -1$, 3, and 4, the 25th harmonic is expected to exhibit a wavefront rotation of −25, 75, and 100 wavelengths, respectively. Remarkably, in all the cases, the harmonic wavefront twist is within 2% of the theoretically expected value: ~−25.01, ~75.01, and ~98.6$\lambda$ for $l_1 = -1$, 3, and 4, respectively. Conclusively, even for such a high topological charge, the harmonic vortex obtained in an extended generation medium retains its helical wavefront during up-conversion, hence, ruling out any disruptive effects from propagation and phase matching.[20,50]

Once the amplitude and phase are experimentally characterized, in order to extract more information about the OAM content of the high-order harmonic beam, we use the Fourier relationship between the topological charge $l$ and the azimuthal angle $\phi$ to retrieve the OAM spectrum as a function of the radial coordinate.[51] The radially integrated OAM spectrum for each case is shown in the right column of Figure 2. Noticeably, a broad distribution with a rich OAM content is observed for all the configurations. Moreover, the OAM spectrum is much broader for $l_{25} = 75$ and 100 than for $l_{25} = -25$. This indicates that even if the overall topological charge indeed follows the linear scaling with the harmonic order ($l_q = ql_1$),[21] the retrieved EUV vortex beams feature a superposition of several OAM modes. This nonpure character of the harmonic beams may come from the azimuthal modulations present in their intensity distribution, since the azimuthal Fourier transform requires cylindrical symmetry to obtain pure OAM modes. However, the lack of perfect symmetry around the principal OAM value (right column of Figure 2) suggests that the IR vortex driver might be contaminated with OAM modes other than the principal one. In fact, the use of a nonpure IR vortex beam has been theoretically proposed as a source of the rich OAM content of harmonic beams due to the highly nonperturbative nature of HHG.[34] To examine if we are under these conditions, we characterized the intensity, wavefront, and OAM content of the IR driving beams.


https://doi.org/10.1021/acsphotonics.1c01768
ACS Photonics 2022, 9, 944−951

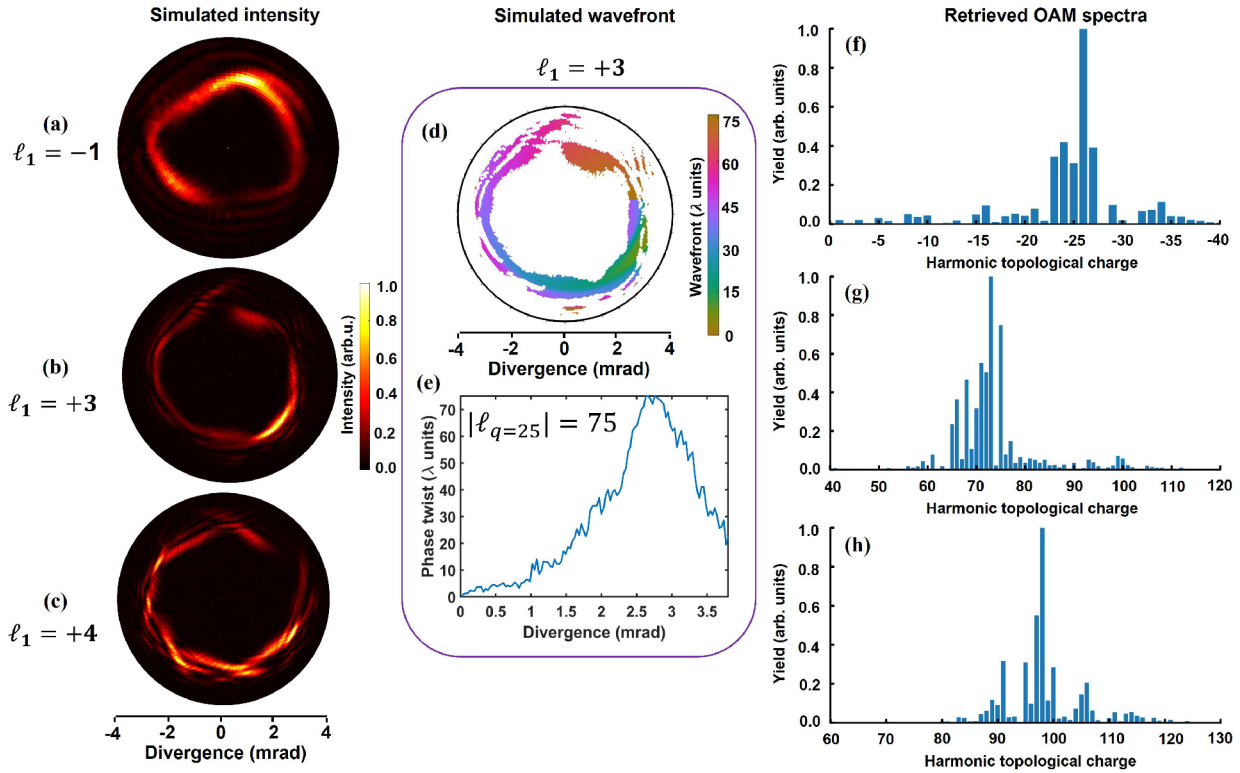


**Figure 4.** HHG OAM simulation results using the experimental vortex driver. We use the experimentally retrieved phase and amplitude of IR vortex beams to simulate HHG in argon. In the left column we show the simulated intensity profiles of the 25th harmonic using our full quantum SFA macroscopic approach for (a) $l_1 = -1$, (b) $l_1 = 3$, and (c) $l_1 = 4$. For a selected case of $l_1 = 3$, we show the simulated wavefront (d) and phase twist (e), expressed in the unit of $\lambda$ as a function of divergence. Note that, for the driving beam of $l_1 = 3$, the wavefront twist of $75\lambda$ is in agreement with the experimental observation (Figure 2b) and represents the expected upscaling of the topological charge with the harmonic order. Again, for the sake of completeness, we show the radially integrated HHG OAM spectra in (f)−(h) for $l_1 = -1$, 3, and 4, respectively. The main OAM contribution channels are the 26th, 73rd, and 98th for $|l_1| = 1$, 3, and 4, respectively, in excellent agreement with the experimental results presented in Figure 2.

## EXPERIMENTAL CHARACTERIZATION OF THE IR VORTEX DRIVING BEAMS

Following the focusing optics, a series of beam samplers guide the driving vortex beam to the IR wavefront sensor, which is located ∼300 mm after the focal plane (see Figure 1 and the Supporting Information). The measured intensity and wavefront of the IR vortex beams at the wavefront sensor plane are presented in the Supporting Information, Figure S1. Additionally, over an extended period, the topological charge measurement shows a deviation of ∼1% or less, indicating the high stability of the driving beams (see the Supporting Information and Figure S2). To obtain the intensity and the wavefront of the IR driving beams at the waist, the complex field reconstructed by the wavefront sensor is numerically backpropagated to the focal plane (see the Supporting Information). In Figure 3 we show the resulting intensity (first column), wavefront (second column) at the waist, and OAM content (third column) for the IR vortex beams with a topological charge of $l_1 = -1$, 3, and 4 (first, second, and third rows, respectively). In addition to the annular intensity profile, the size of the dark spot resulting from the central phase singularity increases with the topological charge, as expected. The merit of our characterization approach can be assessed through an excellent agreement between the backpropagated and experimentally acquired intensity distribution at the waist (see Figure S3 in the Supporting Information). The OAM content presented in the right column shows that, although the driving beams possess high modal purity (∼93.4% for $l_1 = -1$, ∼92.6% for $l_1 = 3$, and ∼92% for $l_1 = 4$), there is a non-negligible contribution from other modes as well.

We note that SPPs are nonideal mode converters offering a limited efficiency,[52] whereas the residual aberrations present in the Gaussian beam can further degrade the mode purity.[53] Even for a high-quality Gaussian input such as the one used in this work (RMS wavefront ∼ $\lambda/32$, see the Supporting Information), the helical beams produced by SPPs are a superposition of numerous Laguerre−Gauss modes. Additionally, as SPPs are designed for a particular wavelength, topological charge dispersion is naturally induced for broadband femtosecond pulses.[54,55] Therefore, SPPs inevitably yield a driver beam comprising a superposition of different OAM modes. For a quantitative comparison, the theoretical OAM mode-conversion efficiency for a 16-segment phase plate of unit topological charge is ∼95%,[54] whereas the experimentally obtained efficiency for $|l_1| = 1$ is ∼93.4%, which is very close to the theoretical estimation.

## SIMULATION OF OAM-DRIVEN HHG USING THE EXPERIMENTAL DRIVING BEAM

The theoretical simulations of the HHG in argon have been computed using the experimentally retrieved IR driving beam, which allows us to obtain a deeper insight into the experimental results. We utilize the experimental driving beam at the waist (Figure 3) as an input to our numerical


https://doi.org/10.1021/acsphotonics.1c01768
ACS Photonics 2022, 9, 944−951

model, which is based on a combination of the extended strong field approximation and the electromagnetic field propagator[56] (see the Supporting Information).

In the first column of Figure 4 we show the simulated intensity profile of the 25th harmonic when driven by the IR drivers presented in Figure 3, for $l_1 = -1$, 3, and 4 (first, second and third row, respectively). First and foremost, we observe a close resemblance between the simulated and the experimental intensity profiles. The complex features of the experimental intensity profiles are well reproduced by the computed results. For the selected case of $l_1 = 3$, we show the wavefront in Figure 4d and the phase twist as a function of the beam divergence in Figure 4e. The simulated phase bears a twist of $75\lambda$, which is in agreement with the experimental observation. In the third column of Figure 4 we show the radially integrated OAM spectrum corresponding to each condition, obtained after performing the Fourier transform of the 25th harmonic along the azimuthal coordinate. The OAM spectrum shows a broad distribution for all the cases, which is in qualitative agreement with the experimental results presented in Figure 2. We also note that for both experimental and simulated results, the topological charges with the largest contributions are the 26th, 73rd, and 98th for $|l_1| = 1$, 3, and 4, respectively. We remark that as the intensity profiles present noncylindrical symmetries, the OAM distribution is very sensitive to the centering reference from where the azimuthal Fourier transform is performed. The distortions and modulations of both numerical and experimental intensity profiles influence the OAM spectrum, since they introduce additional OAM modes that are sensitive to small displacements of the centering reference (see Figure S4 in the Supporting Information). For this reason, we have optimized the centering procedure to obtain the minimum standard deviation in each OAM distribution presented in this work.

## CONCLUSION

We demonstrate the generation of EUV vortex beams with a topological charge of up to 100 through HHG in a noble gas. We use wavefront metrology to fully characterize their intensity and helical wavefront. To the best of our knowledge, this is the first work that demonstrates the successful generation, followed by a complete characterization, of such a high charge vortex structure in the EUV domain. In this sense, the presented results pave the way for the characterization of very high OAM EUV beams, which is a prerequisite for their applications. These results also show that, even in an extended generation medium (15 mm long), the twisted phase of the IR vortex driver is upconverted and preserved during HHG. Consequently, a further long medium can be used to generate intense EUV vortex beams for practical applications. Though the overall wavefront twist confirms a linear upconversion of the topological charge with harmonic order, an in-depth analysis reveals the sensitivity of the EUV OAM to the purity of the driving beam. Even for a highly pure driver of $l_1 = -1$ (~93.4%), a mere contribution of a few percentages from other modes can affect the high-order harmonic OAM spectrum.

From a fundamental point of view, we note that the topological charge carried by an ultrafast vortex beam is limited by its pulse duration.[57] Such a limit for the highest topological charge in our work would correspond to $\sim 10^6$, which is far from our situation due to the relatively long pulse duration of our driving pulse (~40 fs) and the high frequency of the harmonics. However, if several high-order harmonics with the same high OAM charge were synthesized into a subfemtosecond laser pulse, the limits established in ref 57 would be experimentally accessible. Thus, if combined with other techniques to generate high-order harmonics with the same OAM charge,[28] our work would provide a route to experimentally explore the limits of OAM in ultrafast science. From a technological point of view, we demonstrate that the intensity and wavefront of high charge vortex beams can be reliably characterized using the wavefront sensing approach. Note that the techniques that are unable to measure both amplitude and phase profile provide only an averaged OAM value. Thanks to the high resolution of the EUV Hartmann sensor, we can numerically extract the OAM composition of the harmonic vortex beams from the experimentally reconstructed complex field. Our approach can further be extended to obtain the radial mode content using the full Laguerre−Gauss decomposition of the field. This, for instance, can be used to study the effect of intensity and phase matching on the radial mode structure of HHG vortex beams.

The generation and characterization of EUV vortex beams with a large OAM in the high frequency regime paves the way for ultrafast studies of OAM transfer from light to matter at a beam size comparable to the natural spatial scales of electronic dynamics in clusters or molecules.[58] Further studies of tight focusing of such beams are required. Fortunately, the versatility of the HHG process offers different lensless focusing approaches[35,59,60] that could be used to achieve low divergence beams without the need for focusing optics. In this regard, we also note that the EUV wavefront sensing allows for the determination of the HHG beam waist position from the measured wavefront curvature radius, therefore, offering the possibility to investigate the optics-less focusing aspect of high-OAM EUV vortex beams.

## ASSOCIATED CONTENT

### Supporting Information

The Supporting Information is available free of charge at https://pubs.acs.org/doi/10.1021/acsphotonics.1c01768.

(I) Complete description of the experimental setup; (II) Specifications of IR and EUV wavefront sensors; (III) Characterization of the fundamental Gaussian IR beam; (IV) Methodology of wavefront detection and reconstruction for IR and EUV vortex beams; (V) Long-term IR vortex driver stability measurement; (VI) Details on the backpropagation of the IR driver beam field from the detection plane to the waist, which is then used to perform HHG simulations; (VII) Details of the theoretical method for full quantum HHG simulation with macroscopic propagation; and (VIII) Figures S1−S7 that complement the findings in the main text (PDF)

## AUTHOR INFORMATION

### Corresponding Authors

**Alok Kumar Pandey** − *Laboratoire Iréne Joliot-Curie, Université Paris-Saclay, UMR CNRS, F-91898 Orsay Cedex, France;* orcid.org/0000-0003-3755-4843; Email: alok-kumar.pandey@etu.univ-amu.fr

**Alba de las Heras** − *Grupo de Investigación en Aplicaciones del Láser y Fotónica, Departamento de Física Aplicada, Universidad de Salamanca, E-37008 Salamanca, Spain;*

orcid.org/0000-0001-9065-9076;
Email: albadelasheras@usal.es

### Authors

**Tanguy Larrieu** − *Laboratoire Iréne Joliot-Curie, Université Paris-Saclay, UMR CNRS, F-91898 Orsay Cedex, France*
**Julio San Román** − *Grupo de Investigación en Aplicaciones del Láser y Fotónica, Departamento de Física Aplicada, Universidad de Salamanca, E-37008 Salamanca, Spain*
**Javier Serrano** − *Grupo de Investigación en Aplicaciones del Láser y Fotónica, Departamento de Física Aplicada, Universidad de Salamanca, E-37008 Salamanca, Spain;* orcid.org/0000-0003-2093-2000
**Luis Plaja** − *Grupo de Investigación en Aplicaciones del Láser y Fotónica, Departamento de Física Aplicada, Universidad de Salamanca, E-37008 Salamanca, Spain*
**Elsa Baynard** − *Laboratoire Iréne Joliot-Curie, Université Paris-Saclay, UMR CNRS, F-91898 Orsay Cedex, France*
**Moana Pittman** − *Laboratoire Iréne Joliot-Curie, Université Paris-Saclay, UMR CNRS, F-91898 Orsay Cedex, France*
**Guillaume Dovillaire** − *Imagine Optic, 91400 Orsay, France*
**Sophie Kazamias** − *Laboratoire Iréne Joliot-Curie, Université Paris-Saclay, UMR CNRS, F-91898 Orsay Cedex, France*
**Carlos Hernández-García** − *Grupo de Investigación en Aplicaciones del Láser y Fotónica, Departamento de Física Aplicada, Universidad de Salamanca, E-37008 Salamanca, Spain;* orcid.org/0000-0002-6153-2647
**Olivier Guilbaud** − *Laboratoire Iréne Joliot-Curie, Université Paris-Saclay, UMR CNRS, F-91898 Orsay Cedex, France*

Complete contact information is available at: https://pubs.acs.org/10.1021/acsphotonics.1c01768

### Author Contributions

[§]These authors contributed equally to this work. A.K.P., A.H., C.H-G., and O.G. conceived the study; A.K.P. implemented and led the experiment; A.K.P. and O.G. conducted the measurements; E.B. and M.P. ensured the laser operation; G.D. and A.K.P. devised the method and parameters for high-OAM wavefront reconstruction; A.K.P., T.L., and O.G. treated the experimental data; A.H., J.S.R., J.S., L.P., and C.H-G. performed and analyzed the simulations; and A.K.P., A.H., J.S.R., O.G., and C.H-G. wrote the manuscript. All authors discussed results and reviewed the manuscript.

### Funding

European Research Council (851201); Ministerio de Ciencia de Innovación y Universidades, Agencia Estatal de Investigación and European Social Fund (PID2019-106910GB-I00, RYC-2017-22745); Junta de Castilla y León and FEDER Funds (SA287P18); Université Paris-Saclay (2012-0333T-OASIS, 50110000724-OPTX, PhOM REC-2019-074-MAO-HAm); Conseil Régional, Île-de-France (501100003990); and Barcelona Supercomputing Center (FI-2020-3-0013).

### Notes

The authors declare no competing financial interest.

## ■ ACKNOWLEDGMENTS

The project leading to this publication has received funding from the European Research Council (ERC) under the European Union's Horizon 2020 Research and Innovation Program. We acknowledge the computer resources at MareNostrum and the technical support provided by the Barcelona Supercomputing Center. The authors thank CEMOX installation at IOGS, Palaiseau, France, for the design and fabrication of the multilayer optics. We acknowledge the technical support of the IJC Lab staff, specifically, J. Demailly and O. Neveu. We thank D. Gauthier, P. Rebernik Ribic, G. De Ninno, and K. Dorney for fruitful discussions.

## ■ REFERENCES

(1) Rubinsztein-Dunlop, H.; et al. Roadmap on structured light. *J. Opt.* **2017**, *19*, 013001.
(2) Forbes, A.; de Oliveira, M.; Dennis, M. R. Structured light. *Nat. Photonics* **2021**, *15*, 253−262.
(3) Allen, L.; Beijersbergen, M. W.; Spreeuw, R. J. C.; Woerdman, J. P. Orbital angular momentum of light and the transformation of Laguerre-Gaussian laser modes. *Phys. Rev. A* **1992**, *45*, 8185−8189.
(4) Yao, A. M.; Padgett, M. J. Orbital angular momentum: origins, behavior and applications. *Adv. Opt. Photon.* **2011**, *3*, 161−204.
(5) Gahagan, K. T.; Swartzlander, G. A. Optical vortex trapping of particles. *Opt. Lett.* **1996**, *21*, 827−829.
(6) Padgett, M.; Bowman, R. Tweezers with a twist. *Nat. Photonics* **2011**, *5*, 343−348.
(7) Hell, S. W.; Wichmann, J. Breaking the diffraction resolution limit by stimulated emission: stimulated-emission-depletion fluorescence microscopy. *Opt. Lett.* **1994**, *19*, 780−782.
(8) Vicidomini, G.; Bianchini, P.; Diaspro, A. STED super-resolved microscopy. *Nat. Methods* **2018**, *15*, 173−182.
(9) Willner, A. E.; et al. Optical communications using orbital angular momentum beams. *Adv. Opt. Photon.* **2015**, *7*, 66−106.
(10) Wang, J. Advances in communications using optical vortices. *Photonics Res.* **2016**, *4*, B14−B28.
(11) Mair, A.; Vaziri, A.; Weihs, G.; Zeilinger, A. Entanglement of the orbital angular momentum states of photons. *Nature* **2001**, *412*, 313−316.
(12) Fickler, R.; Lapkiewicz, R.; Plick, W. N.; Krenn, M.; Schaeff, C.; Ramelow, S.; Zeilinger, A. Quantum Entanglement of High Angular Momenta. *Science* **2012**, *338*, 640−643.
(13) Schmiegelow, C. T.; Schulz, J.; Kaufmann, H.; Ruster, T.; Poschinger, U. G.; Schmidt-Kaler, F. Transfer of optical orbital angular momentum to a bound electron. *Nat. Commun.* **2016**, *7*, 12998.
(14) De Ninno, G.; et al. Photoelectric effect with a twist. *Nat. Photonics* **2020**, *14*, 554−558.
(15) Fanciulli, M. Observation of magnetic helicoidal dichroism with extreme ultraviolet light vortices. *arXiv:2103.13697 [physics.optics]* **2021**, na.
(16) Wang, X.; Nie, Z.; Liang, Y.; Wang, J.; Li, T.; Jia, B. Recent advances on optical vortex generation. *Nanophotonics* **2018**, *7*, 1533−1556.
(17) Peele, A. G.; McMahon, P. J.; Paterson, D.; Tran, C. Q.; Mancuso, A. P.; Nugent, K. A.; Hayes, J. P.; Harvey, E.; Lai, B.; McNulty, I. Observation of an x-ray vortex. *Opt. Lett.* **2002**, *27*, 1752−1754.
(18) Rebernik Ribič, P. c. v.; et al. Extreme-Ultraviolet Vortices from a Free-Electron Laser. *Phys. Rev. X* **2017**, *7*, 031036.
(19) Lee, J. C. T.; Alexander, S. J.; Kevan, S. D.; Roy, S.; McMorran, B. J. Laguerre-Gauss and Hermite-Gauss soft X-ray states generated using diffractive optics. *Nat. Photonics* **2019**, *13*, 205−209.
(20) Zürch, M.; Kern, C.; Hansinger, P.; Dreischuh, A.; Spielmann, C. Strong-field physics with singular light beams. *Nat. Phys.* **2012**, *8*, 743−746.
(21) Hernández-García, C.; Picón, A.; San Román, J.; Plaja, L. Attosecond Extreme Ultraviolet Vortices from High-Order Harmonic Generation. *Phys. Rev. Lett.* **2013**, *111*, 083602.
(22) Gariepy, G.; Leach, J.; Kim, K. T.; Hammond, T. J.; Frumker, E.; Boyd, R. W.; Corkum, P. B. Creating High-Harmonic Beams with Controlled Orbital Angular Momentum. *Phys. Rev. Lett.* **2014**, *113*, 153901.

(23) Géneaux, R.; Camper, A.; Auguste, T.; Gobert, O.; Caillat, J.; Taïeb, R.; Ruchon, T. Synthesis and characterization of attosecond light vortices in the extreme ultraviolet. *Nat. Commun.* **2016**, *7*, 12583.
(24) Gauthier, D.; et al. Tunable orbital angular momentum in high-harmonic generation. *Nat. Commun.* **2017**, *8*, 14971.
(25) Kong, F.; Zhang, C.; Bouchard, F.; Li, Z.; Brown, G. G.; Ko, D. H.; Hammond, T. J.; Arissian, L.; Boyd, R. W.; Karimi, E.; Corkum, P. B. Controlling the orbital angular momentum of high harmonic vortices. *Nat. Commun.* **2017**, *8*, 14970.
(26) Sanson, F.; et al. Hartmann wavefront sensor characterization of a high charge vortex beam in the extreme ultraviolet spectral range. *Opt. Lett.* **2018**, *43*, 2780−2783.
(27) Paufler, W.; Böning, B.; Fritzsche, S. Tailored orbital angular momentum in high-order harmonic generation with bicircular Laguerre-Gaussian beams. *Phys. Rev. A* **2018**, *98*, 011401.
(28) Dorney, K. M.; Rego, L.; Brooks, N. J.; San Román, J.; Liao, C.-T.; Ellis, J. L.; Zusin, D.; Gentry, C.; Nguyen, Q. L.; Shaw, J. M.; Picón, A.; Plaja, L.; Kapteyn, H. C.; Murnane, M. M.; Hernández-García, C. Controlling the polarization and vortex charge of attosecond high-harmonic beams via simultaneous spin-orbit momentum conservation. *Nat. Photonics* **2019**, *13*, 123−130.
(29) Rego, L.; Dorney, K. M.; Brooks, N. J.; Nguyen, Q. L.; Liao, C.-T.; San Román, J.; Couch, D. E.; Liu, A.; Pisanty, E.; Lewenstein, M.; Plaja, L.; Kapteyn, H. C.; Murnane, M. M.; Hernández-García, C. Generation of extreme-ultraviolet beams with time-varying orbital angular momentum. *Science* **2019**, *364*, eaaw9486.
(30) Ferray, M.; L'Huillier, A.; Li, X. F.; Lompre, L. A.; Mainfray, G.; Manus, C. Multiple-harmonic conversion of 1064 nm radiation in rare gases. *J. Phys. B: At., Mol. Opt. Phys.* **1988**, *21*, L31−L35.
(31) Schafer, K. J.; Yang, B.; DiMauro, L. F.; Kulander, K. C. Above threshold ionization beyond the high harmonic cutoff. *Phys. Rev. Lett.* **1993**, *70*, 1599−1602.
(32) Basistiy, I.; Bazhenov, V.; Soskin, M.; Vasnetsov, M. Optics of light beams with screw dislocations. *Opt. Commun.* **1993**, *103*, 422−428.
(33) Dholakia, K.; Simpson, N. B.; Padgett, M. J.; Allen, L. Second-harmonic generation and the orbital angular momentum of light. *Phys. Rev. A* **1996**, *54*, R3742−R3745.
(34) Rego, L.; Román, J. S.; Picón, A.; Plaja, L.; Hernández-García, C. Nonperturbative Twist in the Generation of Extreme-Ultraviolet Vortex Beams. *Phys. Rev. Lett.* **2016**, *117*, 163202.
(35) Rego, L.; Brooks, N. J.; Nguyen, Q. L. D.; Román, J. S.; Binnie, I.; Plaja, L.; Kapteyn, H. C.; Murnane, M. M.; Hernández-García, C. Necklace-structured high-harmonic generation for low-divergence, soft x-ray harmonic combs with tunable line spacing. *Sci. Adv.* **2022**, *8*, eabj7380.
(36) Soskin, M. S.; Gorshkov, V. N.; Vasnetsov, M. V.; Malos, J. T.; Heckenberg, N. R. Topological charge and angular momentum of light beams carrying optical vortices. *Phys. Rev. A* **1997**, *56*, 4064−4075.
(37) Harris, M.; Hill, C.; Vaughan, J. Optical helices and spiral interference fringes. *Opt. Commun.* **1994**, *106*, 161−166.
(38) Hickmann, J. M.; Fonseca, E. J. S.; Soares, W. C.; Chávez-Cerda, S. Unveiling a Truncated Optical Lattice Associated with a Triangular Aperture Using Light's Orbital Angular Momentum. *Phys. Rev. Lett.* **2010**, *105*, 053904.
(39) Alperin, S. N.; Niederriter, R. D.; Gopinath, J. T.; Siemens, M. E. Quantitative measurement of the orbital angular momentum of light with a single, stationary lens. *Opt. Lett.* **2016**, *41*, 5019−5022.
(40) Reddy, S. G.; Permangatt, C.; Prabhakar, S.; Anwar, A.; Banerji, J.; Singh, R. P. Divergence of optical vortex beams. *Appl. Opt.* **2015**, *54*, 6690−6693.
(41) Starikov, F. A.; Kochemasov, G. G.; Kulikov, S. M.; Manachinsky, A. N.; Maslov, N. V.; Ogorodnikov, A. V.; Sukharev, S. A.; Aksenov, V. P.; Izmailov, I. V.; Kanev, F. Y.; Atuchin, V. V.; Soldatenkov, I. S. Wavefront reconstruction of an optical vortex by a Hartmann-Shack sensor. *Opt. Lett.* **2007**, *32*, 2291−2293.
(42) Leach, J.; Keen, S.; Padgett, M. J.; Saunter, C.; Love, G. D. Direct measurement of the skew angle of the Poynting vector in a helically phased beam. *Opt. Express* **2006**, *14*, 11919−11924.
(43) Stoklasa, B.; Motka, L.; Rehacek, J.; Hradil, Z.; Sánchez-Soto, L. L. Wavefront sensing reveals optical coherence. *Nat. Commun.* **2014**, *5*, 3275.
(44) Denoeud, A.; Chopineau, L.; Leblanc, A.; Quéré, F. Interaction of Ultraintense Laser Vortices with Plasma Mirrors. *Phys. Rev. Lett.* **2017**, *118*, 033902.
(45) Gauthier, D.; Kaassamani, S.; Franz, D.; Nicolas, R.; Gomes, J.-T.; Lavoute, L.; Gaponov, D.; Février, S.; Jargot, G.; Hanna, M.; Boutu, W.; Merdji, H. Orbital angular momentum from semiconductor high-order harmonics. *Opt. Lett.* **2019**, *44*, 546−549.
(46) Ghimire, S.; DiChiara, A. D.; Sistrunk, E.; Agostini, P.; DiMauro, L. F.; Reis, D. A. Observation of high-order harmonic generation in a bulk crystal. *Nat. Phys.* **2011**, *7*, 138−141.
(47) Levecq, X. J.-f., Harms, F. Device for analysing a wavefront with enhanced resolution. U.S. Patent US7301613, 2007.
(48) Esashi, Y.; Liao, C.-T.; Wang, B.; Brooks, N.; Dorney, K. M.; Hernández-García, C.; Kapteyn, H.; Adams, D.; Murnane, M. Ptychographic amplitude and phase reconstruction of bichromatic vortex beams. *Opt. Express* **2018**, *26*, 34007−34015.
(49) Fu, S.; Zhang, S.; Wang, T.; Gao, C. Pre-turbulence compensation of orbital angular momentum beams based on a probe and the Gerchberg-Saxton algorithm. *Opt. Lett.* **2016**, *41*, 3185−3188.
(50) Hernández-García, C.; Román, J. S.; Plaja, L.; Picón, A. Quantum-path signatures in attosecond helical beams driven by optical vortices. *New J. Phys.* **2015**, *17*, 093029.
(51) Yao, E.; Franke-Arnold, S.; Courtial, J.; Barnett, S.; Padgett, M. Fourier relationship between angular position and optical orbital angular momentum. *Opt. Express* **2006**, *14*, 9071−9076.
(52) Beijersbergen, M.; Coerwinkel, R.; Kristensen, M.; Woerdman, J. Helical-wavefront laser beams produced with a spiral phaseplate. *Opt. Commun.* **1994**, *112*, 321−327.
(53) Ohland, J. B.; Eisenbarth, U.; Roth, M.; Bagnoud, V. A study on the effects and visibility of low-order aberrations on laser beams with orbital angular momentum. *Appl. Phys. B: Laser Opt.* **2019**, *125*, 202.
(54) Longman, A.; Fedosejevs, R. Mode conversion efficiency to Laguerre-Gaussian OAM modes using spiral phase optics. *Opt. Express* **2017**, *25*, 17382−17392.
(55) Ruffato, G.; Massari, M.; Romanato, F. Generation of high-order Laguerre-Gaussian modes by means of spiral phase plates. *Opt. Lett.* **2014**, *39*, 5094−5097.
(56) Hernández-García, C.; Pérez-Hernández, J. A.; Ramos, J.; Jarque, E. C.; Roso, L.; Plaja, L. High-order harmonic propagation in gases within the discrete dipole approximation. *Phys. Rev. A* **2010**, *82*, 033432.
(57) Porras, M. A. Upper Bound to the Orbital Angular Momentum Carried by an Ultrashort Pulse. *Phys. Rev. Lett.* **2019**, *122*, 123904.
(58) Picón, A.; Benseny, A.; Mompart, J.; Vázquez de Aldana, J. R.; Plaja, L.; Calvo, G. F.; Roso, L. Transferring orbital and spin angular momenta of light to atoms. *New J. Phys.* **2010**, *12*, 083053.
(59) Wikmark, H.; Guo, C.; Vogelsang, J.; Smorenburg, P. W.; Coudert-Alteirac, H.; Lahl, J.; Peschel, J.; Rudawski, P.; Dacasa, H.; Carlström, S.; Maclot, S.; Gaarde, M. B.; Johnsson, P.; Arnold, C. L.; L'huillier, A. Spatiotemporal coupling of attosecond pulses. *Proc. Natl. Acad. Sci. U.S.A.* **2019**, *116*, 4779−4787.
(60) Quintard, L.; Strelkov, V.; Vabek, J.; Hort, O.; Dubrouil, A.; Descamps, D.; Burgy, F.; Péjot, C.; Mével, E.; Catoire, F.; Constant, E. Optics-less focusing of XUV high-order harmonics. *Sci. Adv.* **2019**, *5*, eaau7175.


https://doi.org/10.1021/acsphotonics.1c01768
ACS Photonics 2022, 9, 944−951